Proc. Estonian Acad. Sci. Eng., 2007, **13**, 3, 215–233

https://doi.org/10.3176/eng.2007.3.04

An experimental investigation of the oscillatory boundary layer around the breaking point

Toomas Liiv

Tallinn University of Technology, Ehitajate tee 5, 19086 Tallinn, Estonia; toomas@corson.ee

Received 14 February 2007, in revised form 20 June 2007

Abstract. The article describes experimental investigation of the turbulent oscillatory boundary layer in the vicinity of the wave breaking point. Measurements were carried out on the inclined bottom in 29 cross-sections, of which 3 are investigated in the current paper. These cross-sections are chosen so that they include the breaking point. The semi-logarithmic plots of dimensionless velocity profiles were plotted on the basis of laser Doppler anemometer measurements. The velocity distributions in breaking waves are essentially different from those observed in steady flows or in oscillatory flows in rectangular *U*-tubes.

Key words: oscillatory flow, breaking wave, boundary layer, velocity distribution.

1. INTRODUCTION

One of the most interesting problems, associated with the modelling of oscillatory flows, is the description of the boundary layer flow field and shear stress during the wave period. Different authors have proposed various empirical solutions and performed numerous experiments that in many cases involve uniform flow over a horizontal bottom. One has to distinguish boundary layers in flows with a variation of the water depth due to the bottom change from the case with the horizontal bottom.

Today there are several quasi-stationary models that describe processes in the boundary layer in case of oscillatory flow over horizontal bottom. These models can roughly be divided into three groups.

The simplest model assumes that the velocity distribution in the boundary layer is logarithmic during the whole period of oscillation, while the boundary layer thickness varies. Viability of these models depends on the roughness of the bottom. The first of these classical models was presented in [1].

The second type of models [2–6] assumes that the flow distribution during the horizontal oscillatory flow resembles the flow distribution in a laminar oscillatory flow. These models are derived to describe the harmonic component of the flow. The velocity distribution in this case is approximated as

$$u(z,t) = A\omega[1 - D_1(z)]e^{i\omega t}, \tag{1}$$

where

$$D_1(z) = \exp\left[-(1+i)\frac{z}{\sqrt{2\nu/\omega}}\right]. \tag{2}$$

Here $u(z,t)$ is the variation of the velocity over the vertical coordinate z at time t, A is the amplitude of motion, ω is frequency, $D_1(z)$ is the velocity defect function for smooth laminar flow and ν is kinematic viscosity. Stokes length, δ_S, for the turbulent flow both for rough and smooth boundaries, is expressed through

$$\delta_S = \sqrt{2\nu/\omega}, \tag{3}$$

which describes the vertical scale of the velocity distribution.

The velocity defect function D_1 can be expressed as

$$D_1 = \exp[-(1+i)(z/z_1)^p]. \tag{4}$$

The parameters z_1 and p are tabulated and depend on the relative roughness and Reynolds number. When the relative roughness is greater than about 0.01, Eq. (1) together with Eq. (4) describe well both turbulent and transitional boundary layers [7].

The third type of models to solve the boundary layer problems are eddy viscosity based models together with the equation of motion

$$\rho\frac{\partial u}{\partial t} = -\frac{\partial p}{\partial x} + \frac{\partial \tau}{\partial z}, \tag{5}$$

where p is pressure, ρ is density, x is horizontal coordinate and τ is the shear stress.

When vertical accelerations are neglible in comparison with the acceleration of gravity and due to that the shear stresses vanish outside the boundary layer, Eq. (5) can be written as

$$\rho\frac{\partial}{\partial t}(u - u_\infty) = \frac{\partial \tau}{\partial z}. \tag{6}$$

Here u_∞ is the velocity infinitely far away from the boundary. Assuming that eddy viscosity ν_t depends only on z, but not on t, shear stresses can be expressed as $\tau = \nu_t(\partial u/\partial z)$ and Eq. (6) can be rewritten as

$$\frac{\partial}{\partial t}(u-u_\infty)=\frac{\partial}{\partial z}\left(\nu_t\frac{\partial u}{\partial z}\right). \tag{7}$$

Different type of eddy viscosity models have been developed in [8] assuming a three-layer eddy viscosity distribution. But Kajura's model [8] is based on the information, obtained from the steady boundary layer investigations. Simplifying this model and abandoning the inner layer, we obtain the Grant and Madsen model [9,10]

$$\nu_t = ku^* z, \qquad 0 < z < \infty. \tag{8}$$

Here $k \cong 0.4$ is the von Karman coefficient and u^* is the shear velocity.

All mathematical models of coastal processes need some parameters that allow us to describe the velocity distribution in the boundary layer during the breaking process. Using eddy viscosity models, the velocity distribution in the oscillatory boundary layer was mathematically derived in [8–10]. Brevik [11] proposed another model to determine the two-layer eddy viscosity distribution. He simplified the model by omitting the inner layer. Rodi [12] considers all possible eddy viscosity schemes, including the k–ε scheme, for solving turbulent boundary layer problems. Christensen and Deigaard [13] calculated the flow fields, large eddies and turbulent kinetic energy fields of plunging and spilling breakers.

A model that takes into account also the time dependence of eddy viscosity is described in [14]. Only a few of such models are satisfactory in predicting the magnitude and phase of the simple velocity $u(z,t)$ in case of the horizontal bottom.

The models that describe the processes on the inclined bottom usually also take into account the generation of bottom ripples that are responsible for the generation of vorticity in the bottom boundary layer. Already in 1982, several numerical methods for rounded ripple profiles were published [15,16], which describe shear stress on the wall adequately. Blondeaux and Vittori [17] have presented different methods of vorticity generation and prediction of suspended sediment around these vortices. Different types of eddy viscosity models have been used to describe oscillatory flow on the inclined bottom [18]. Feddersen et al. [19] measured the shear coefficient, bottom roughness and wave breaking on the ocean beach. Wave breaking on the natural beach and its boundary layer has also been investigated [20].

Theoretical results [14] agree well with the measurements [21] of the near bottom velocity in an oscillating water tunnel. Jensen et al. [7,22] measured the turbulent boundary layer in an oscillatory water tunnel at large Reynolds numbers studying smooth and rough bottoms. Flush mounted hot film sensors were used for direct measurements of the bottom velocities.

All mathematical models that describe bottom boundary layer flows use data obtained in oscillatory flows in pressure pipes [21]. Investigation of the flow structure and boundary layer in free surface flows started with the introduction of the laser Doppler anemometer (LDA) technology. First papers were published in

the 1980s [23]. Both vertical and horizontal coordinates of the velocity were measured.

Most of the models of the oscillatory boundary layer make assumptions, based on experimental investigations [21]. Experiments have shown that the velocity infinitely far away from the solid boundary, u_∞, varies sinusoidally in time and the shear stress $\tau(0,t)$ follows the same trend with a slight phase shift (Fig. 1). This phase shift is initiated by the hydrodynamic processes in the wave. The same phase lag was also noticed in [24].

The velocity profiles for different values of ωt that correspond to Fig. 1 are presented in Fig. 2.

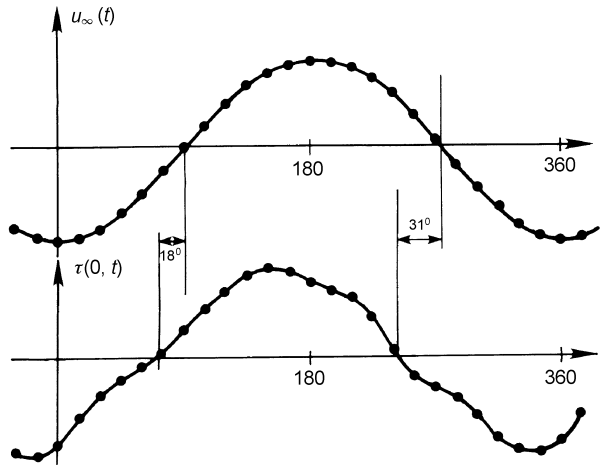

Fig. 1. Time variations of the bed shear stress $\tau(0,t)$ for rough turbulent flow over relatively small roughness elements [1]; horizontal axes present ωt.

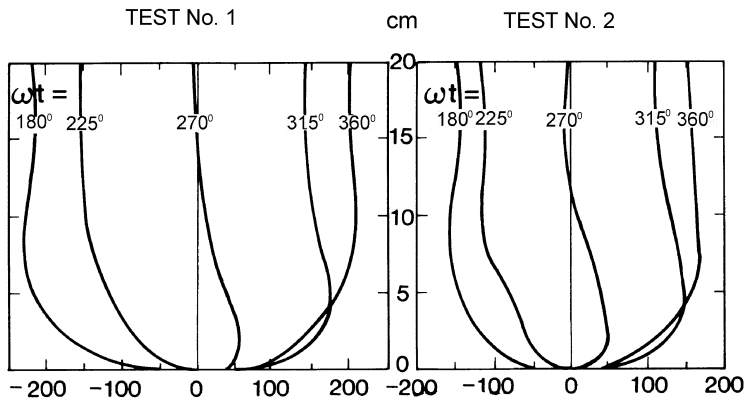

Fig. 2. Instantaneous velocities $u(z,t)$ plotted against elevation from top of the roughness elements. Numbers on the curves refer to the phase ωt of the free stream velocity $A\omega\sin\omega t$ [1].

Figure 1 shows that the velocity near the bed turns back before the free stream velocity. The maximum value of the velocity is not on the free surface, but near the bottom, at the level of about ¼ of the stream height.

Most models that calculate the time-dependent flow velocity distribution in the boundary layer use the non-dimensional velocity profiles derived in [7,22]. These experiments were conducted in a U-tube with rectangular cross-section. The free stream velocity changes according to the pattern $A\omega\sin\omega t$. Figure 3 shows the semilog arithmic plot of the mean velocity distribution. The orbital amplitude over the boundary layer was $A = 3.1\,\text{m}$ and the oscillation period $T = 9.72\,\text{s}$. The dimensionless distance y^+ from the bed and the dimensionless velocity u^+ were calculated as

$$y^+ = \frac{z}{\nu}, \qquad u^+ = \frac{\langle u(z,t)\rangle}{\langle u^*(t)\rangle}, \tag{9}$$

where $\langle\cdot\rangle$ is the ensemble average.

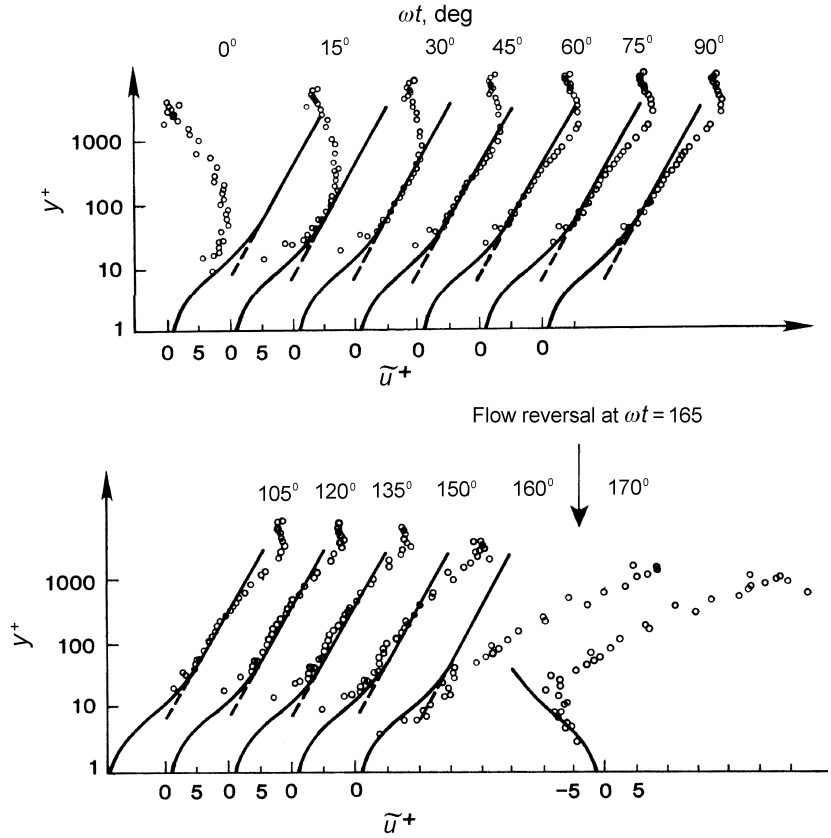

Fig. 3. Dimensionless velocity profiles for smooth turbulent oscillatory flows at different phases of the free stream velocity $A\omega\sin\omega t$ (after [7]).

As the flow is in the boundary layer on the smooth flat surface, these values do not change along the flow.

Here and below u^+ tends to the logarithmic distribution

$$u^+ = (1/k)\ln y^+ + 5 \tag{10}$$

at large values of y^+.

Many experimental works are dedicated to the determination of oscillatory velocity distribution, both for two- and three-dimensional flows and for smooth and rough boundaries, for example [25–32]. Here it is suitable also to mention that systematic investigations of the oscillatory boundary layer flow around the breaking point have been performed and therefore the basis for boundary layer calculations is taken from [6].

Cox et al. [33] investigated shear stresses, measured in the wave flume on the inclined bottom profile. Krstic and Fernando [34] investigated the effect of artificial roughness on the bottom boundary layer. Bryan et al. [35] used Sontek Acoustic Velocimeter to measure wave energy and energy dissipation in the breaking waves on the coast of New Zealand.

The aim of the present article is qualitative comparison of the above described models with experimental results, obtained in the wave flume of the Tallinn University of Technology [36–38].

2. RESULTS ON THE OSCILLATORY BOUNDARY LAYER

The following results on experimental investigation of oscillatory flow were obtained during experiments, described in [24]. The goal was to compare the measured velocity distribution in the boundary layer with velocity distributions, used in mathematical models. The experiments were carried out in a wave flume with a surf zone of a constant slope of 1 to 17. The aim of the investigation was to get an insight into the flow structure and different hydrodynamic processes in the vicinity of the wave breaking point. The velocity field inside the breaking waves was measured with the two-component argon-ion laser Doppler anemometer with an output power of 1.3 W. Forward scatter mode was used throughout the experiments. As the LDA system allows measurement only at one point, the measurements were repeated over the vertical for all 29 profiles and 1852 measuring points. The total number of wave cycles, sampled at each measuring point, was 151. The data processing procedures and main results of investigations are described in [24]. The main attention in the study was focused on the determination of the velocity field inside the breaking wave, especially in the area close to the bottom of the surf zone, where data was collected with the vertical step of 1 mm. The closest measuring point to the bottom was considered to show the bottom shear velocity. The reasoning behind this assumption is that the laser beams, measuring the horizontal velocity component, enter the flume under an angle (Fig. 4). Thus it was possible to project the measuring volume to

the very bottom of the flume. It can also be said that the height of the first measuring point above the bottom is equal to half of the shorter half-axis of the measuring volume. The dimensions of the measuring volume can be calculated as

$$\delta_x = \frac{4F\lambda}{\pi E D_L \cos\frac{\theta}{2}}, \qquad \delta_z = \frac{4F\lambda}{\pi E D_L \sin\frac{\theta}{2}}, \tag{11}$$

where δ_x and δ_z are the lengths of the shorter and longer axis of the measuring volume, respectively, λ is the wavelength of the laser beam, and other notations are shown in Fig. 4. This gives the value of the shorter half-axis 0.12 mm, which gives the same precision as the precision of mounting the hot film probe. The horizontal velocity, measured closest to the bottom, was taken to be the shear velocity u^*.

In order to evaluate the values of the shear velocity, measured in the described way, calibration calculations were made using the method proposed in [39]. This method permits the evaluation of the values of the shear velocity in case of shallow water wave action. The analysis showed that the results achieved were satisfactory and the coincidence of the measurement data with existing information was good.

Figure 5 presents experimentally obtained dimensionless velocity profiles for smooth turbulent oscillatory flow at different wave phases. Only three profiles of the 29 measured ones are presented. In Fig. 5 and further the following notations are used: $\bar{\eta}$ is the average surface elevation, $<U>$ is the ensemble-averaged horizontal velocity, C is the wave phase velocity, x_b is the horizontal coordinate of the breaking point, y_b is the water depth at the breaking point and h_b is the average water depth at the breaking point. The profiles correspond to the profile before breaking, at the breaking point and immediately after breaking. The value of ωt is chosen so that ωt = 0 in the wave trough.

The lines coloured pink, green and dark blue represent the backflow from the beach and the lines coloured black, brown and light blue represent the onflow towards the beach. The flow profiles during backflow resemble the classical steady flow profiles in open channels. During onflow towards the beach the velocity profiles are remarkably different from the steady open channel flow. The measurements show that, during the onflow, the horizontal velocity of the water particles is larger in the near-bed zone and in the layers close to the water surface than in the intermediate layers. This can be explained with the backflow of water that decelerates the water particles in the intermediate zone to the level that it forms almost a homogeneous flow pattern in the given zone.

Figure 6 presents an example of measured time series of the shear velocity u^* before processing; only four of the measured 151 periods are presented. The data is from a profile with coordinates $(x - x_b)/h_b = 0.09$. It can be seen that the value of u^* fluctuates considerably around its mean value. The data processing smoothened the curve and also got rid of drop-outs between $\omega t = 360$ and $\omega t = 720$ deg. Data processing is described in detail in [24].

In order to verify the results presented in Fig. 6, a comparison was made with the results obtained by Jensen et al. [22] with constant temperature anemometer (CTA) in an oscillating U-tube. In case of the Reynolds number $Re = 3.4\times10^6$, the shear velocity was found to be $u^* = 0.73$ m/s. For the present case with *Re* = 3.0×10^6, the shear velocity was 0.62 m/s. Since the two velocities are close to each other, this result confirms that the given approach to measuring the shear velocity is adequate. A comparison of the values of τ_0/ρ was also made with the results presented in [28]. The overall shapes of τ_0/ρ agreed well for both experiments, but as the resolution of the graphs in [28] was low, an exact comparison was not possible.

Figures 7 to 9 present the ensemble-averaged variation of non-dimensional shear velocities and the corresponding surface elevations during one wave period in the same cross-sections as in Fig. 5.

The most distinctive feature is that both the shear velocity and the wave height increase towards the breaking point and decrease after breaking.

The analysis of the shear velocity in the boundary layer shows that the obtained results substantially differ from the results obtained in the oscillatory pressure tube [7,22]. This can be explained firstly with the inclined surface of the used experimental setup and secondly with the open boundary on the water surface that allows more adequate representation wave movement.

Figures 10 to 15 present profiles of the dimensionless velocity u^+ at different phases of the wave breaking; $y^+ = h\langle u\rangle/\nu$ is the dimensionless distance from bed and u^+ is the ratio of local velocity to the friction velocity (see Eq. (9)).

The scale of the axes was selected so that the results are comparable with the results of [7], presented in Fig. 3. As mentioned before, the phase 0 corresponds to the wave trough. The same choice of the wave phase was also used in Fig. 3.

In Figs. 10 to 15, steady flow velocity distributions near the wall are shown for comparison. They are calculated as follows. It is assumed that very near to the wall there is a viscous sublayer with linear velocity distribution

$$\frac{u}{u_*} = \frac{u^* y}{\nu}. \tag{12}$$

At some distance from the boundary the turbulent velocity profile is described as

$$\frac{u}{u_*} = 2.5 \ln \frac{u^* y}{\nu} + 5.5. \tag{13}$$

Between these two zones there is a transition zone, where

$$3.5 < u^* y/\nu < 30. \tag{14}$$

Previous investigations have shown that in case of a stationary flow, the dominant stresses for the flow in the viscous sublayer are viscous stresses, whereas in the core region turbulent stresses prevail.

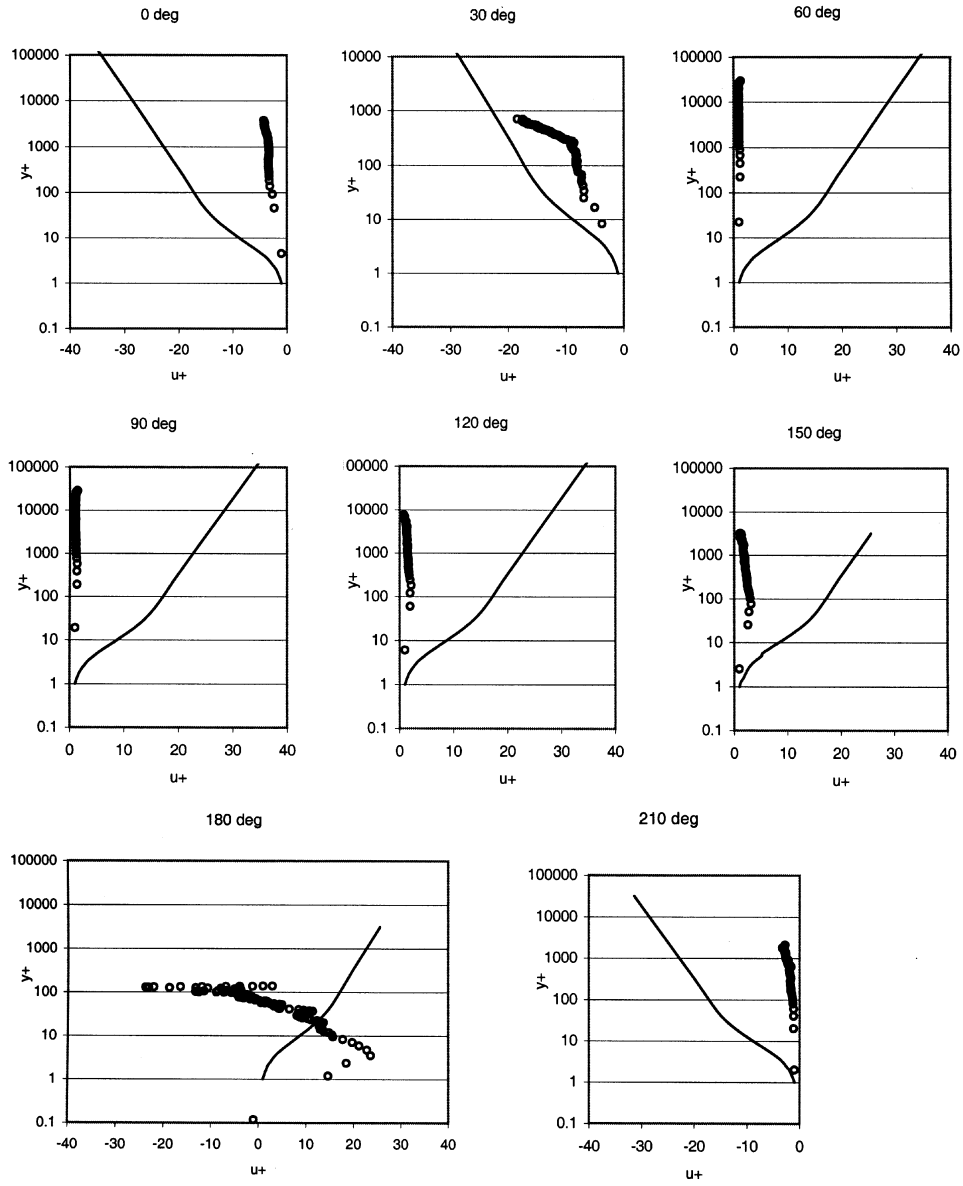

Fig. 10. Dimensionless velocity profiles of $u+$ at different phases of the wave breaking, section $(x - x_b)/h_b = -2.36$; circles show experimental points, solid line indicates the calculated velocity profile in the assumption of the stationary flow.

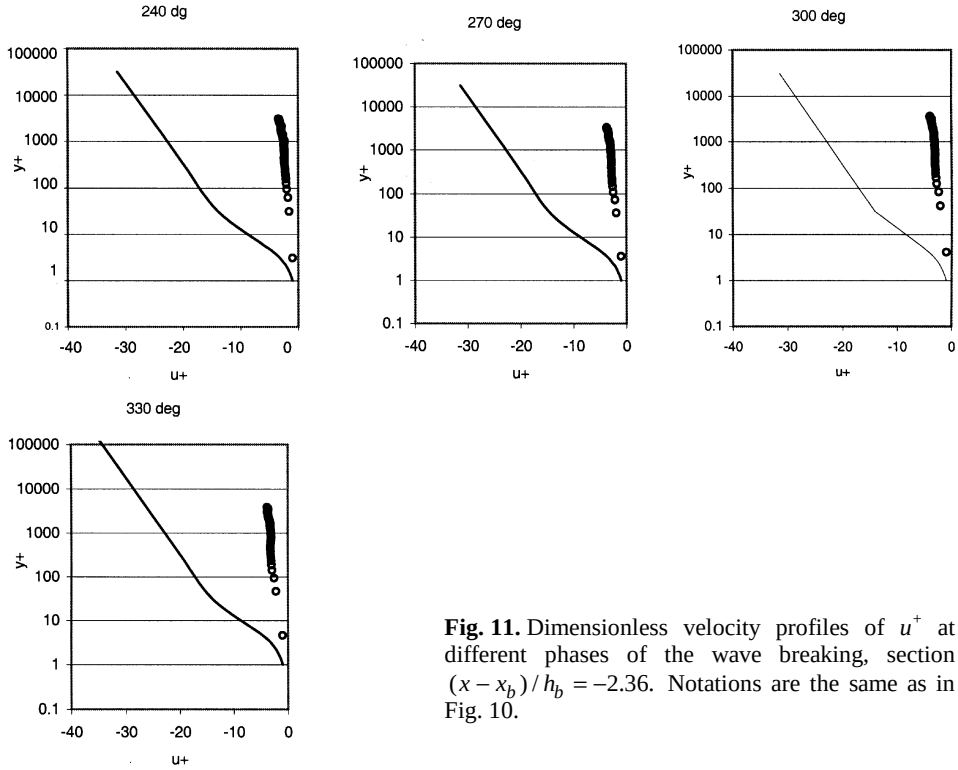

Fig. 11. Dimensionless velocity profiles of u^+ at different phases of the wave breaking, section $(x - x_b)/h_b = -2.36$. Notations are the same as in Fig. 10.

The flow situation in the present experimental run was completely different from the flow in a U-tube with a constant cross-sectional area. The present investigation considers oscillatory flow with a free surface on the inclined bottom. Besides, the flow incorporates relatively rapid change of the cross-sectional area of the flow due to wave breaking, and the generation of two-phase environment (air–water) on the wave crest and after the breaking point over the whole cross-sectional area. In addition to the local inertial forces, the flow is influenced by convective inertial forces.

The profiles of the dimensionless velocity u^+ (Eq. (9)) in Figs. 10 to 15 are presented for different phase angles with a step of 30 deg. Depending on the flow direction, the stationary flow profile (Eqs. (12) and (13)) is plotted either on the right (flow towards the coast) or on the left (flow towards the deep water) side of the vertical axis. Again the value of 0 deg corresponds to the lowest surface elevation in the wave trough. It can be seen from the figures that flow is directed towards the shore between 60 and 180 deg. At the breaking point the flow reversal is somewhat later, at 210 deg. At other phases the flow is directed towards the deep water. The data shows that the value of $y^+ = y^+(u^+)$ changes only a little both for $(x - x_b)/h_b = -2.36$ and $(x - x_b)/h_b = 0.09$. The only exceptions are flow reversals at 15 and 90 deg for $(x - x_b)/h_b = -2.36$ and also at 15 and 105 deg for $(x - x_b)/h_b = 0.09$.

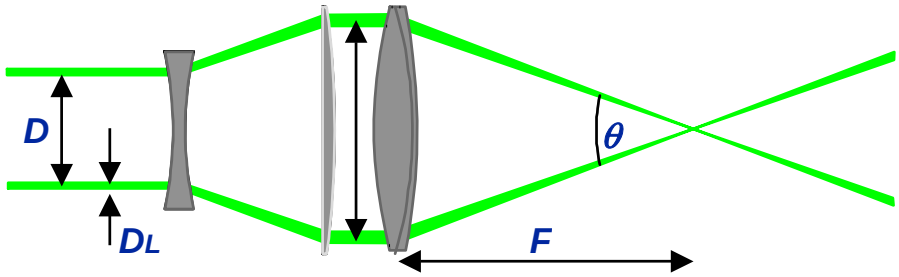

Fig. 4. Measurement scheme.

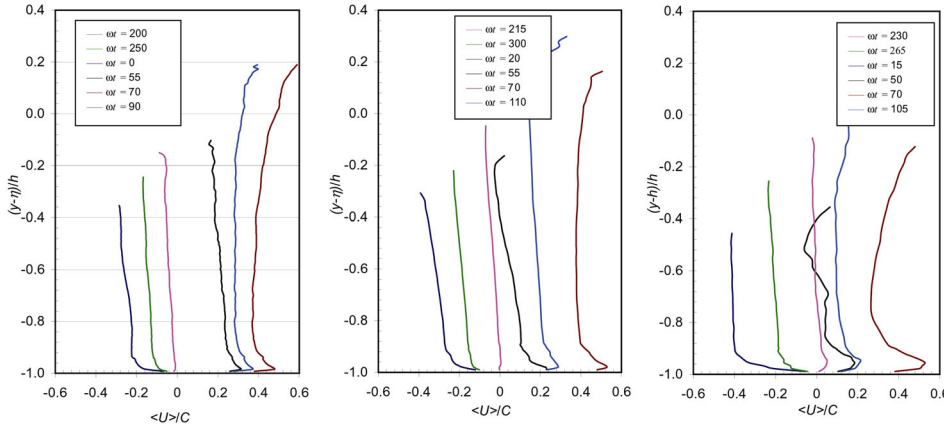

(a) (b) (c)

Fig. 5. Dimensionless velocity profiles at different wave phases: (a) – $(x - x_b)/h_b = -2.36$; (b) – $(x - x_b)/h_b = 0.09$; (c) – $(x - x_b)/h_b = 2.17$.

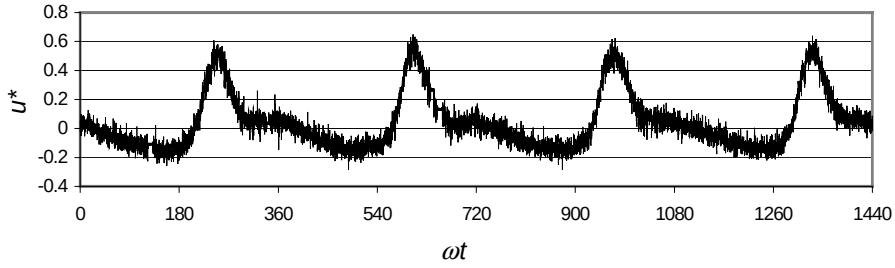

Fig. 6. Measured time series of the shear velocity before data processing.

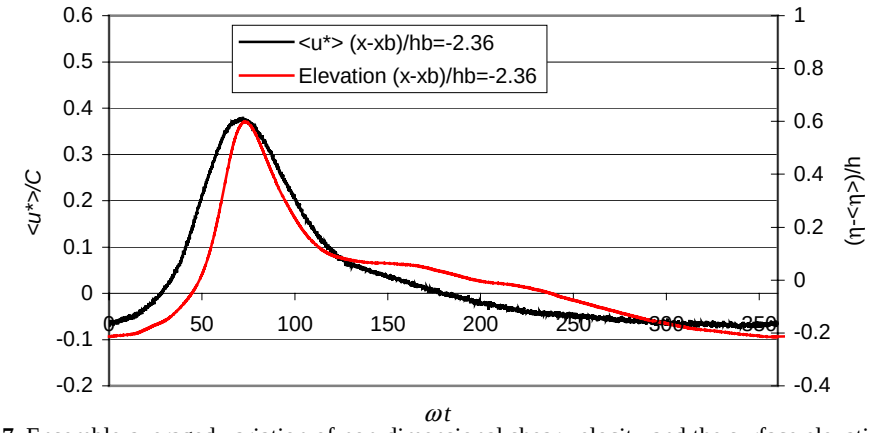

Fig. 7. Ensemble-averaged variation of non-dimensional shear velocity and the surface elevation at $(x - x_b)/h_b = -2.36$.

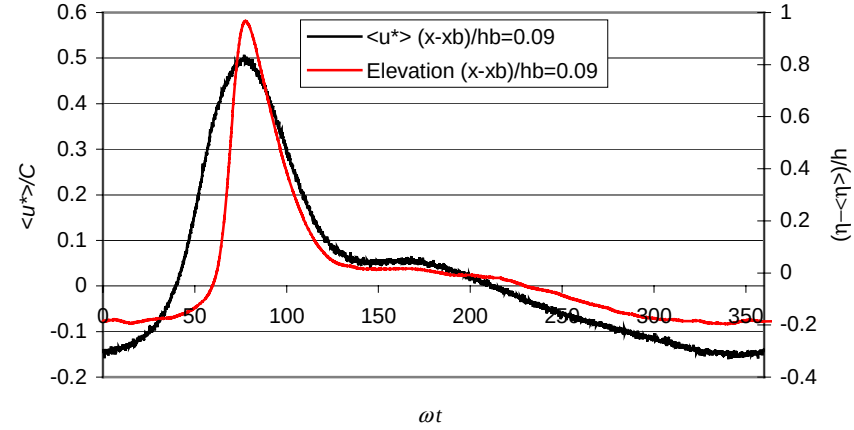

Fig. 8. Ensemble-averaged variation of non-dimensional shear velocity and the surface elevation at $(x - x_b)/h_b = 0.09$.

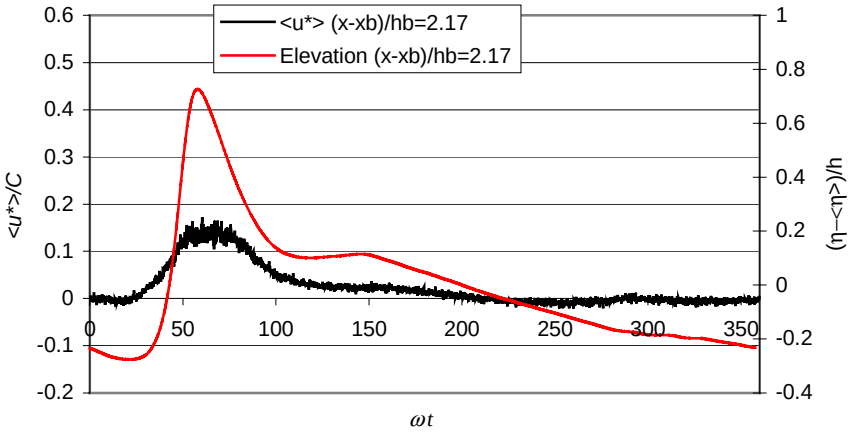

Fig. 9. Ensemble averaged variation of non-dimensional shear velocity and the surface elevation at $(x - x_b)/h_b = 2.17$.

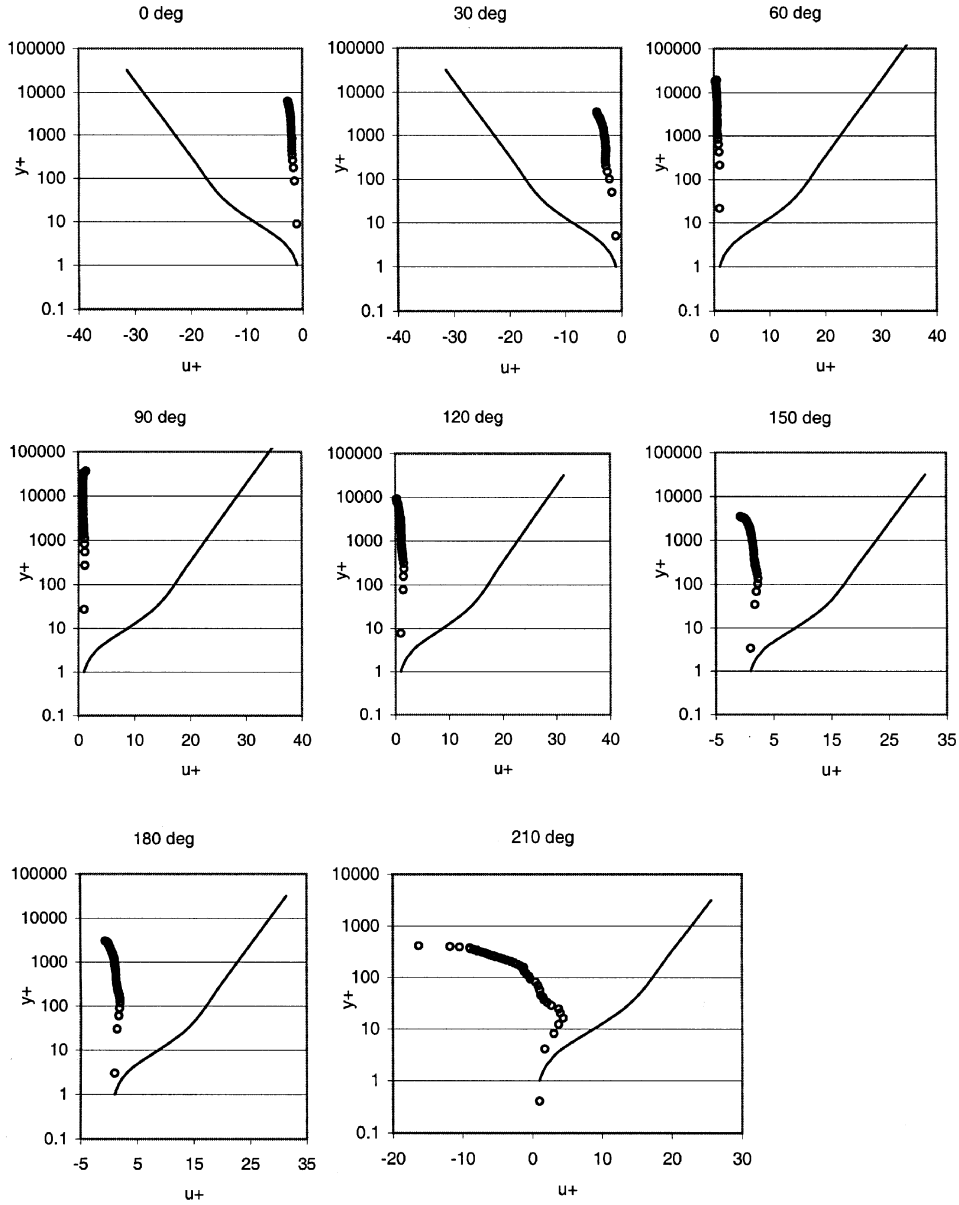

Fig. 12. Dimensionless velocity profiles of $u+$ at different phases of the wave breaking, section $(x - x_b)/h_b = 0.09$. Notations are the same as in Fig. 10.

The experimental results prove that the flow reversal starts at the top of the water column and spreads gradually downwards to the bottom. This phenomenon is best illustrated in Fig. 10 at 90 deg, where the onflow in the wave crest meets the backflow on the bottom. The velocity profiles are almost uniform in Figs. 10 to 13, except for the wave phases at which the flow reverses. Close inspection of

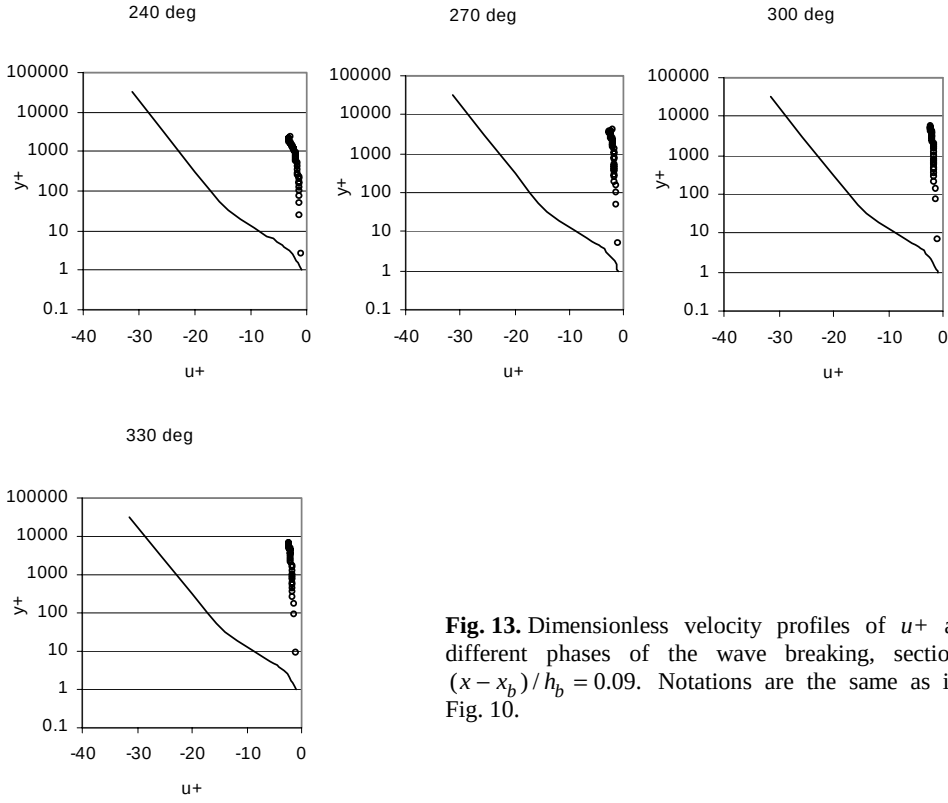

Fig. 13. Dimensionless velocity profiles of $u+$ at different phases of the wave breaking, section $(x - x_b)/h_b = 0.09$. Notations are the same as in Fig. 10.

the values of u^+ reveals that it varies between 1 and 2 during the flow towards the shoreline and between 1 and 3.5 during backflow. This suggests that in comparison with the stationary flow, different processes govern the development of the boundary layer flow under breaking waves.

There are two possible agents that may contribute to almost uniform profiles of u^+. Experiments in pressure pipes [40] have shown that during strong local accelerations, the value of u^+ stays constant over the whole cross-section. The ensemble-averaged horizontal accelerations in the present experiment at certain phases of the wave cycle were found to be up to 1.3 times the acceleration due to gravity. This suggests that the acceleration of water particles and the associated local inertia forces keep the dimensionless flow profile uniform. The second agent that contributes to the uniform profile, especially during the flow phases towards the shoreline, is strong mixing processes due to the overturning of the wave crest. The water particles with high values of the momentum are plunged to the bottom and there they transfer their energy to all the particles.

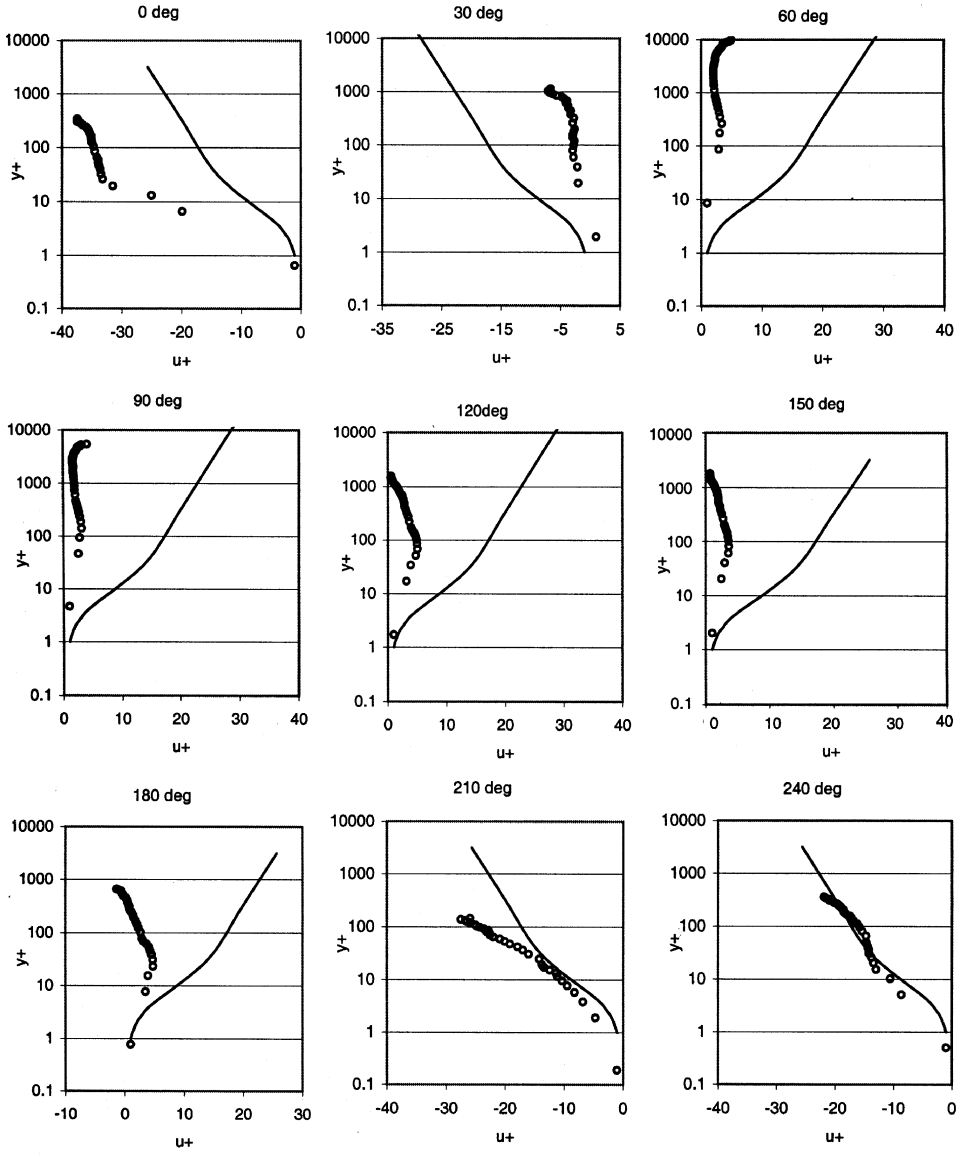

Fig. 14. Dimensionless velocity profiles of $u+$ at different phases of the wave breaking, section $(x - x_b)/h_b = 2.17$. Notations are the same as in Fig. 10.

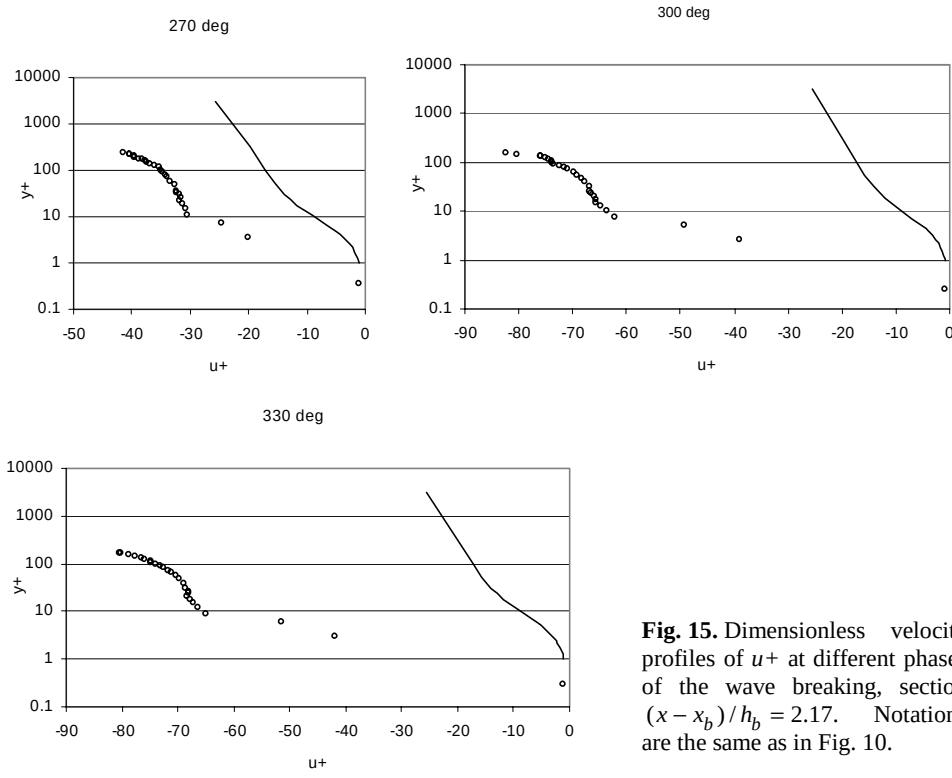

Fig. 15. Dimensionless velocity profiles of $u+$ at different phases of the wave breaking, section $(x - x_b)/h_b = 2.17$. Notations are the same as in Fig. 10.

The situation is totally different in case of the profile after the breaking point at $(x - x_b)/h_b = 2.17$ (Figs. 14 and 15). Although the flow towards and away from the shoreline occurs still at the same wave phases, the behaviour of u^+ is different from the previous cross-sections. During the flow phases towards the shoreline, the dimensionless flow profile is nearly uniform, with the value of u^+ ranging from 1 to 5. It is quite interesting to follow the mixing process. The area of the high value of local velocity in comparison to the friction velocity moves towards the bottom from $y^+ = 10\,000$ at $\omega t = 60°$ to $y^+ = 50$ at $\omega t = 180°$.

The behaviour of the flow during backflow, with ωt varying from 210° to 0°, suggest that the forces, which govern the flow here, are different from the ones that dominated the backflow in the previous investigated profiles. First of all, it must be noted that at $(x - x_b)/h_b = 2.17$ the height of the water column in the approaching wave crest is 2.5 times larger than in the wave trough. This brings along the issues of convective accelerations and flow continuity. These problems were not an issue in the profiles before and during breaking, where the wave crest had a sufficient supply of water in the relatively deep wave trough preceding the wave. The flow behaviour after the flow has reversed at $\omega t = 210°$, resembles very much the stationary open channel flow. The same conclusion can also be made by observing in Fig. 5a the rightmost green line. It resembles very

much the analogous curve for the open channel flow. The next phases are crucial in the development of flow in the current profiles. The approaching wave crest draws the water particles into the crest, generating a strong flow from the relatively shallow wave trough. This phenomenon can be well seen in Fig. 15. The ratio $\langle u(z;t)\rangle \big/ \langle u^*(t)\rangle$ exceeds the "usual" value from 5 up to 40 times.

3. CONCLUSIONS

The present study focused on the investigation of the behaviour of the turbulent oscillatory boundary layer in the oscillatory wave movement in the area immediately before, during and after the breaking process. The measurements of velocities inside the breaking wave were carried out in 29 profiles around the wave breaking point.

As a result of the experiments, the semi-logarithmic plots of the dimensionless velocity distribution $u^+ = \langle u(z;t)\rangle \big/ \langle u^*(t)\rangle$ were calculated for all profiles. The results show that the stationary open channel flow velocity distribution fails to describe the flow under breaking wave although previous investigations have proven that it describes the oscillatory flow in U-shaped flow tunnels relatively well. The two velocity distributions are completely different from each other.

It was also found that the flow pattern after breaking differs from the patterns observed before and during breaking.

ACKNOWLEDGEMENT

The author wishes to thank Corson Consulting for financial support.

REFERENCES

1. Jonsson, I. G. Wave boundary layers and friction factors. In *Proc. 10th International Conference Coastal Engineering*. Tokyo, 1966, 127–148.
2. Kalkanis, G. Turbulent flow near an oscillating wall. *Beach Erosion Board, Technical Memo 97*, 1957.
3. Kalkanis, G. Transportation of bed material due to wave action. *US Army C E R C, Technical Memo 2*, 1964.
4. Sealth, J. F. A. Turbulent oscillatory flow over rough beds. *J. Fluid Mech.*, 1987, **182**, 369–409.
5. Nielsen, P. On the structure of oscillatory boundary layers. *Coastal Eng.*, 1985, **9**, 261–276.
6. Nielsen, P. *Coastal Bottom Boundary Layers and Sediment Transport*. World Scientific, New Jersey, London, 2005.
7. Jensen, B. L. Experimental investigation of turbulent oscillatory boundary layers. Series Paper 45, Institute of Hydrodynamics and Hydraulic Engineering (ISVA), Technical University of Denmark, 1989.
8. Kaijura, K. A model of the bottom boundary layer in water waves. *Bull. Earthquake Res. Inst.*, 1968, **46**, 75–123.
9. Grant, W. D. and Madsen, O. S. Combined wave and current interaction with a rough bottom. *J. Geophys. Res.*, 1979, **87**, 469–481.

10. Grant, W. D. and Madsen, O. S. Movable bed roughness in unsteady oscillatory flow. *J. Geophys. Res.*, 1982, **87**, 469–481.
11. Brevik, I. Oscillatory rough turbulent boundary layers. *J. Waterway Port Coastal Ocean Division, ASCE*, 1981, **107**, 175–188.
12. Rodi, W. *Turbulence Models and Their Application in Hydraulics*. International Association for Hydraulic Research, Delft, 1980.
13. Christensen, E. D. and Deigaard, R. Large eddy simulation of breaking waves. *Coastal Eng.*, 2001, **42**, 53–86.
14. Trowbridge, J. and Madsen, O. S. Turbulent wave boundary layers, I. Model formulation and first order solution. *J. Geophys. Res.*, 1984, **89**, 7989–7997.
15. Sealth, J. F. A. Velocities and shear stresses in wave-current flows. *J. Geophys. Res.*, 1991, **96**, 15237–15244.
16. Sealth, J. F. A. The suspension of sand by waves. *J. Hydraulic Res.*, 1982, **20**, 439–452.
17. Blondeaux, P. and Vittori, G. Oscillatory flow and sediment motion over a rippled bed. In *Proc. 22nd International Conference Coastal Engineering*. Delft, 1990, 2186–2199.
18. Xiuying Xing, M. E. Wave bottom boundary layer physics and bed load sediment transport in nearshore. Master Thesis, The Ohio State University, 2004.
19. Feddersen, F., Gallagher, E. L., Elgar, S. and Guza, R. T. The drag coefficient, bottom roughness, and wave breaking in the nearshore. *Coastal Eng.*, 2003, **48**, 189–195.
20. Trowbridge, J. H. and Agrawal, Y. C. Glimpses of a wave boundary layer. *J. Geophys. Res.*, 1995, **100**, 729–743.
21. Jonsson, I. G. and Carlsen, N. A. Experimental and theoretical investigations in an oscillatory turbulent boundary layer. *J. Hydraulic Res.*, 1976, **14**, 45–60.
22. Jensen, B. L., Sumer, B. M. and Fredsoe, J. Turbulent oscillatory boundary layers at high Reynolds numbers. *J. Fluid Mech.*, 1989, **206**, 265–297.
23. Stieve, M. J. F. Velocity and pressure field of spilling breakers. *Coastal Eng.*, 1980, **25**, 547–566.
24. Liiv, T. and Lagemaa, P. The variation of the velocity and turbulent kinetic energy field in the wave in the vicinity of the breaking point. Forthcoming.
25. Nadaoka, K. and Kondoh, T. Laboratory measurements of velocity field structure in the surf zone by LDV. *Coastal Eng. Japan*, 1982, **25**, 125–145.
26. Lin, P. and Liu, P. L.-F. Turbulence transport, vorticity dynamics and solute mixing under plunging breaking waves in surf zone. *J. Geophys. Res.*, 1998, **103**, 15677–15694.
27. Pedersen, C., Deigaard, R. and Sutherland, J. Measurements of the vertical correlation in turbulence under broken waves. *Coastal Eng.*, 1998, **35**, 231–249.
28. Arnskov, M. M., Fredsoe, J. and Sumer, B. M. Bed shear stress measurements over smooth bed in three dimensional wave-current motion. *Coastal Eng.*, 1993, **20**, 277–316.
29. Stansell, P. Experimental investigation of wave breaking criteria based on wave phase speeds. *J. Phys. Oceanogr.*, 2002, **32**, 1269–1283.
30. Rogers, B. D. and Dalrymple, R. A. SPH modelling of breaking waves. In *Proc. 29th International Conference Coastal Engineering*. Lisbon, 2004, 1147–1157.
31. Liu, P. C. and Babanin, A. V. Using wavelet spectrum analysis to resolve breaking events in the wind wave time series. *Ann. Geophys.*, 2004, **22**, 3335–3345.
32. Sugihara, Y., Tsumori, H. and Takasaki, A. Experimental investigation of turbulent boundary layer beneath a wind-driven surface. In *Proc. 37th International Liege Colloquium on Ocean Dynamics*. Liege, 2005.
33. Cox, D. T., Kobayashi, N. and Okayasu, A. Bottom shear stress in the surf-zone. *J. Geophys. Res.*, 1996, **101**, 337–348.
34. Krstic, R. V. and Fernando, H. J. S. The nature of rough-wall oscillatory boundary layers. *J. Hydraulic Res.*, 2001, **39**, 655–666.
35. Bryan, K. R., Black, K. P. and Gorman, R. M. Spectral estimates of dissipation rate within and near the surf zone. *J. Phys. Oceanogr.*, 2003, **33**, 979–993.

36. Liiv, T. An experimental investigation of the breaking wave characteristics in coastal regions. In *Proc. International Conference on Coastal and Port Engineering in Developing Countries, COPEDEC IV*. Rio de Janeiro, 1995, vol. 3, 2334–2343.
37. Liiv, T. Investigation of turbulence in a plunging breaker wave. *Proc. Estonian Acad. Sci. Eng.*, 2001, **7**, 58–78.
38. Liiv, U. and Liiv, T. Shear investigations of the breaking waves in the flume. In *Proc. 3rd International Conference on Hydro-Science and -Engineering*. Cottbus, Berlin, 1998, CD-ROM, 12 p.
39. Shin, S. Determination of the shear velocities, the bottom roughness and friction factors. Publications of the Oregon State University, Swash Zone Turbulence Group, Report 2, 2004, 15 p.
40. Liiv, U. Unsteady pipe flow transition to turbulence under constant acceleration. In *Proc. 10th Asian Congress of Fluid Mechanics*. Sri Lanka, 2004, CD-ROM, 7 p.

Ostsilleeruva piirikihi eksperimentaalne uurimine laine murdepunkti ümbruses

Toomas Liiv

Lainetusega kaasneva ostsilleeruva voolamise modelleerimisel on üheks tähtsamaks ja suurt praktilist huvi pakkuvaks probleemiks piirikihis tekkivate kiirusväljade muutuste kirjeldamine laineperioodi jooksul. Läbi aegade on selle küsimuse lahendamiseks välja töötatud mitmesuguseid matemaatilisi mudeleid ja teostatud hulgaliselt katseid, mis enamikul juhtudel on aga seotud horisontaalse põhjaga ühtlase voolamisega. Artiklis on kirjeldatud ostsilleeruva piirikihi eskperimentaalse uurimise tulemusi looduslikke olusid modelleerival sileda-põhjalisel kaldpinnal laine murdepunkti ümbruses.